nature geoscience

LETTERS

PUBLISHED ONLINE: 28 APRIL 2013 | DOI: 10.1038/NGEO1802

Andean structural control on interseismic coupling in the North Chile subduction zone

Marta Béjar-Pizarro[1,2]*, Anne Socquet[3], Rolando Armijo[1], Daniel Carrizo[4], Jeff Genrich[5] and Mark Simons[5]

Segmentation can influence the extent of earthquake rupture and event magnitude[1]: large megathrust earthquakes result from total rupture of relatively continuous segments of the subduction interface[2–5]. Segmentation is attributed to variations in the frictional properties of the seismogenic zone or to topographic features on the down-going plate[6–9]. Structures in the overriding plate may also influence segmentation[10–13], but their importance has been dismissed. Here, we investigate the links between interface segmentation at the North Chile seismic gap[14] and a crustal-scale fault structure in the overriding plate that forms a coastal scarp of about 1 km in height[10,15]. We use satellite interferometric synthetic aperture radar (InSAR) and Global Positioning System (GPS) data to measure interseismic surface deformation between 2003 and 2009 and compare the deformation with rupture extent during well-documented earthquakes[5,16–18]. From these data we infer the degree of coupling and segmentation at depth. We find that along a 500-km-long segment, the base of the strongly coupled seismogenic zone correlates with the line of the surface coastal scarp and follows the outline of the Mejillones Peninsula. This correlation implies that large-scale structures in the overriding plate can influence the frictional properties of the seismogenic zone at depth. We therefore suggest that the occurrence of megathrust earthquakes in northern Chile is controlled by the surface structures that build Andean topography.

Understanding factors that limit the extent of seismic rupture is important for both risk mitigation and for understanding physical processes governing the behaviour of seismogenic faults. Devastating megathrust earthquakes in Chile in 2010 and Japan in 2011 ruptured fault segments that were documented to be at least partially coupled before the earthquake, while ruptures terminated in regions that were inferred to be relatively uncoupled[3,4,7,19]. So it seems crucial to evaluate interseismic coupling and its spatial variation in seismic gaps to assess seismic potential. Growing evidence indicates that the structure and geometry of the subduction contact influences fault segmentation and coupling. The occurrence of geometrical complexity at the subduction contact can generate fractures organized in damage zones extending into the upper plate and may modify the seismogenic behaviour of the plate interface (for example, creating low-coupled aseismic barriers). Geometrical barriers are generally attributed to subduction of structures carried by the subducting plate (for example, oceanic ridges, seamounts; refs 8,9,20), whereas the possible role of tectonic structures in the upper plate is ignored. It has been suggested that strong coupling occurs at the oceanward forearc region of the subduction interface, with main asperities correlating well with subsiding forearc basins[11,12,21]. So it is important to determine tectonic features controlling the boundary between the oceanward forearc and the landward forearc regions. In North Chile, we examine the extent to which the spatial distribution of interseismic coupling on the subduction correlates with major Andean structures observed in the upper plate, particularly those controlling the coastline.

The North Chile seismic gap (Fig. 1) extends ~500 km along the Andean subduction and has not experienced any great megathrust earthquake since the 1868 and 1877 events ($\geq M_w$ 8.5; ref. 14). In 2007, the Tocopilla M_w 7.7 earthquake occurred in the southern portion of the gap. Associated coseismic slip (~1–2 m) was confined to the deeper (30–50 km) part of the subduction interface, leaving the shallow part unbroken[18]. Nazca/South America subduction, converging at ~66 mm yr^{-1} in the gap (ref. 22) has elsewhere generated several megathrust earthquakes and devastating tsunamis (for example, the M_w 9.5, 1960 Valdivia or M_w 8.8, 2010 Maule earthquakes). Over the longer term, subduction process has also driven tectonic shortening of the upper plate (that is, the Andean orogeny). The Central Andes is located adjacent to the North Chile seismic gap, and marked by the occurrence of the Altiplano plateau (Fig. 1). The Andean subduction margin represents a total vertical relief reaching ~13 km, from the trench to the high peaks of the Western Cordillera, and is characterized by two major topographic steps. The first step corresponds to the Central Depression, bounded to the west by a ~1,000-m-high coastal scarp, which extends ~500 km along the coastline, slightly obliquely to the trench (Fig. 1). This feature implies recent coastal uplift and requires an active fault structure of similar scale, probably reaching the seafloor near the coast[10]. The second topographic step is formed by the Altiplano plateau, separated from the Central Depression by the 3-km-high west Andean front. That feature seems to be associated with a large-scale east-dipping thrust zone parallel to the subduction zone, responsible for crustal shortening, thickness increase and uplift of the Western Cordillera[23]. Thus the tectonics of the forearc in the North Chile seismic gap region indicates that Andean structures of the overriding plate may be interacting with the subduction processes at relatively shallow, possibly seismogenic, depths[10,24].

Here, we document along-dip and along-strike segmentation of subduction in North Chile using InSAR and continuous

[1]Institut de Physique du Globe de Paris, Sorbonne Paris Cité, Univ. Paris Diderot, UMR 7154 CNRS, F-75005 Paris, France, [2]InSARlab Geohazards InSAR laboratory, Geoscience Research Deptartment, Geological Survey of Spain, Alenza 1, 28003, Spain, [3]Université Joseph Fourier—Grenoble I, OSUG—Observatoire des Sciences de l'Univers de Grenoble, ISTerre—Institut des Sciences de la Terre Maison des Géosciences 1381, rue de la Piscine 38400—Saint Martin d'Heres, France, [4]Departamento de Geofísica, Facultad de Ciencias Físicas y Matemáticas, Universidad de Chile, Blanco Encalada 2002, Santiago, Chile, [5]Seismological Laboratory, Division of Geological and Planetary Sciences, California Institute of Technology, Pasadena, California 91125, USA. *e-mail: mbejarpi@geo.ucm.es.

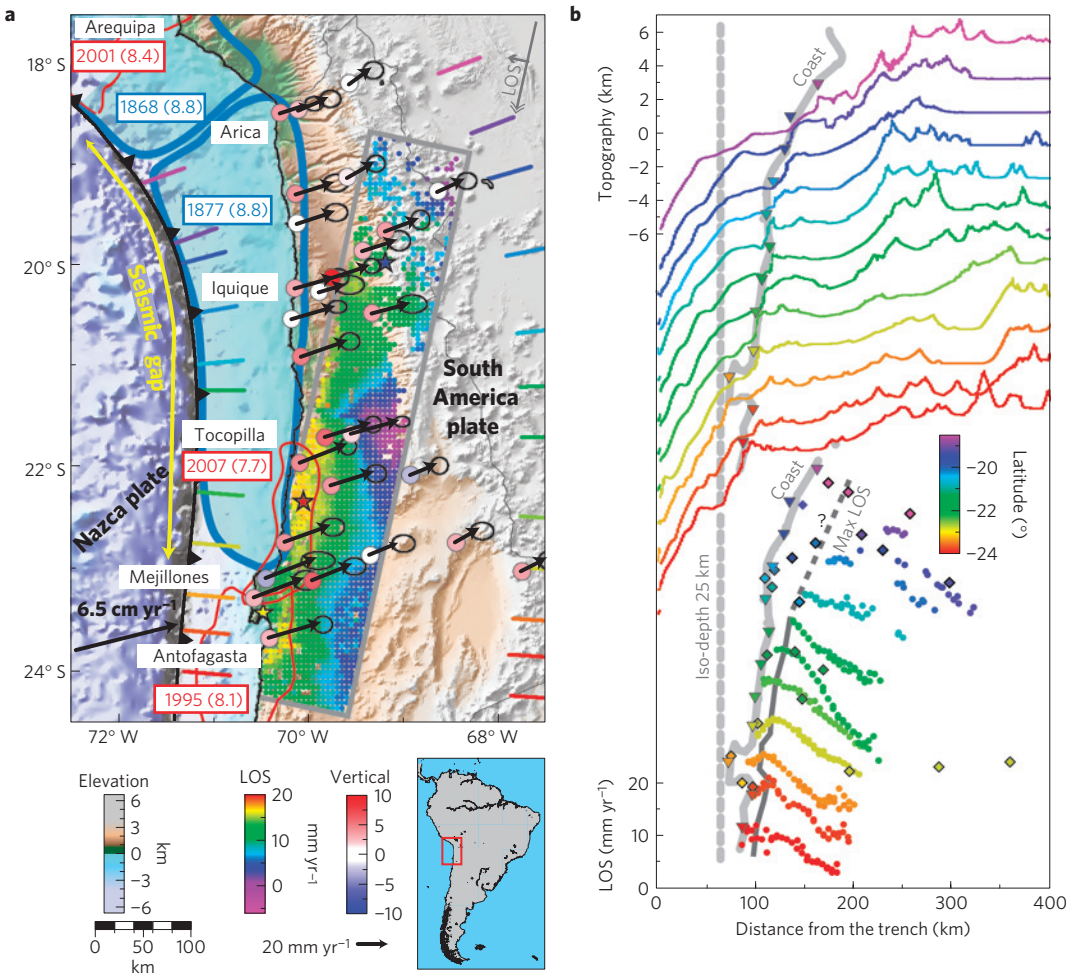

Figure 1 | Interseismic strain measured by InSAR and cGPS. a, Coloured map showing InSAR velocities in LOS (grey arrow), GPS velocities (black arrows, horizontal; coloured dots, vertical), and rupture areas, dates and magnitudes of historic (blue) and instrumental (red) earthquakes. **b**, Cross-sections normal to the trench, sorted and colour-coded by latitude. Top: bathymetric and topographic profiles. Bottom: InSAR (dots) and cGPS (diamonds) velocities projected in LOS. Light grey dashed line, projection of 25 km of iso-depth on a slab dipping 15°. Inverted triangles and light grey line, coastline location. Dark grey line, location of maximum in LOS displacement. (Supplementary Figs S9–S11).

GPS (cGPS) measurements of surface deformation during the interseismic period. We use time series from 29 continuous GPS stations (CAnTO and LIA-MdB networks) to estimate interseismic velocities for the period 2003–2009 (Methods and Supplementary Fig. S1). The horizontal velocity field referenced to South America is characterized by vectors subparallel to Nazca–South America convergence, with magnitudes decreasing with distance from the trench (Fig. 1), indicating that the upper plate is compressed by interseismic loading. The vertical velocity field shows uplift almost everywhere, implying that coupling across the subduction interface does not extend far under the continent[25]. The GPS network precisely measures the broad scale deformation field and the interseismic coupling, but fails to resolve their fine spatial variations. GPS is complemented by a data stack of 18 SAR interferograms which provide continuous spatial coverage of the velocity field for the period 2003–2009 (Fig. 1). The main challenge associated with InSAR processing in this area is to retrieve the long-wavelength tiny interseismic signal that is masked in raw interferograms by atmospheric fringes. Methods and Supplementary Information explain how InSAR data were flattened and corrected for atmospheric tropostatic delays using an empirical approach based on the local correlation between the phase delay and the topography.

The InSAR and cGPS interseismic deformation fields are consistent with each other (Figs 1–3). The maximum displacement in the satellite's line of sight (LOS, ~20° from the vertical) indicates approximately the map projection of the lower limit of the coupled area across the subduction interface, providing us with an image of the 'locked' seismogenic zone (Fig. 1). A series of E–W sections across the InSAR strain rate field shows between 24°–19° S latitude the locked zone widening northwards, parallel to the coast (Fig. 1). The lower limit of coupling also seems to mimic the coastline around the Mejillones Peninsula. The evidence thus indicates a possible mechanical relationship between structures beneath the coast (controlling its shape) and the interseismic coupling across the subduction interface (Figs 1 and 3). The velocity field can be compared with simple forward models (back-slip) of interseismic deformation[25], where the base of the coupled area is either parallel to the trench, as in previously proposed models[5,16,26,27], or parallel to the coast (Fig. 2). Models with coupling parallel to the coastline explain most of the deformation field variance (~80%), whereas models with a constant locking depth (coupling parallel to the trench) fail to reproduce the observed deformation field south of 21° S (see Supplementary Information). Formal inversions of our interseismic velocity field yield a compatible coupling pattern for the subduction interface, with a rather coupled shallow zone extending from the trench to ~30 km depth beneath the coastline, and a transition zone with lower coupling between

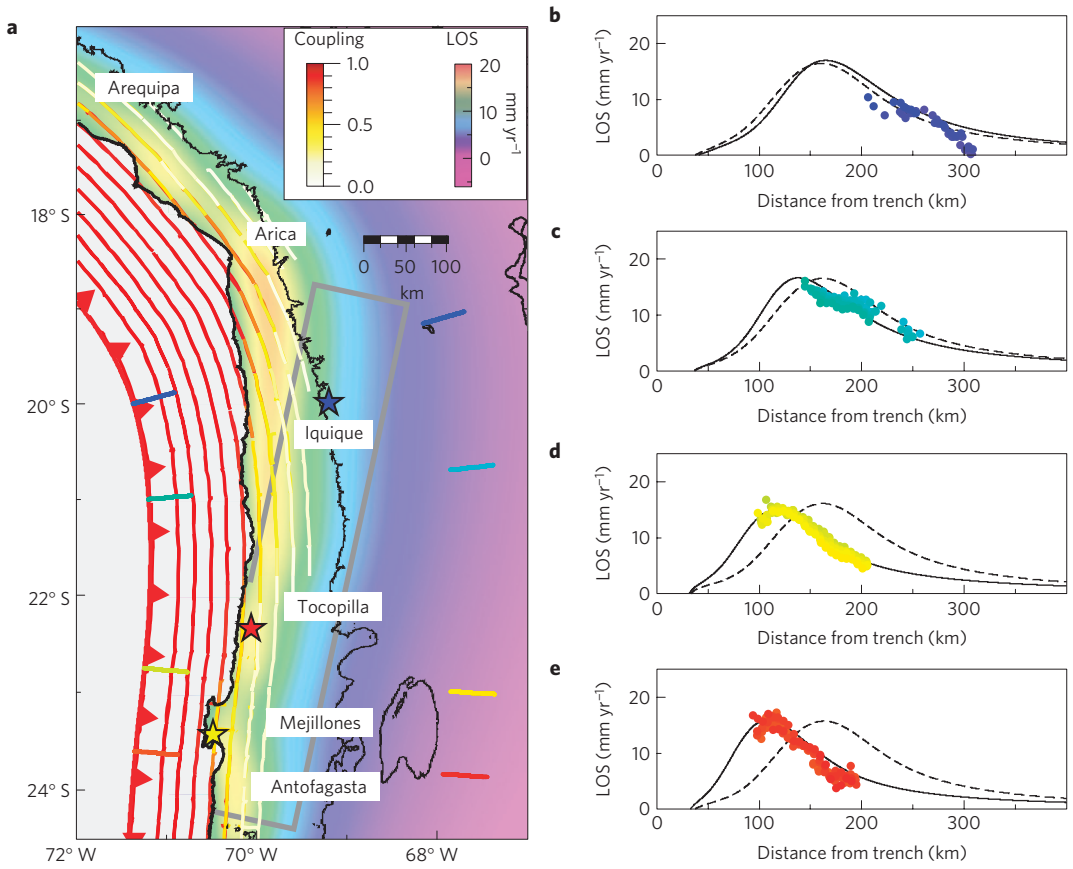

Figure 2 | Synthetic LOS velocities predicted by a coupling model. a, Forward interseismic model where the base of the locked zone follows the coastline. Red-yellow contours, surface projection of the subduction interface iso-depths coloured by coupling value. Rainbow map, predicted LOS velocities. Grey rectangle, spatial limits of our InSAR data. Black contour, altitude 2,500 m. **b**–**e**, Measured and predicted LOS velocities along the equivalent colour-coded profiles identified in **a**. Coloured dots, measured LOS velocities; solid black lines, LOS velocities predicted by the model in **a**; dashed black lines, LOS velocities predicted by a model fully coupled until 30 km depth (Supplementary Figs S13–S15).

30 and 50 km depth (Figs 3 and 4, Supplementary Figs S18 and S19). As the bottom of the coupled zone follows the coast, it deepens northwards, while the coupling coefficient diminishes north of 20.5° S. Whereas coupling near the trench is poorly resolved, the lateral variation of the bottom part of the coupled zone is remarkably well constrained by our data (Supplementary Figs S20 and S21).

Coupling across the subduction interface can be compared in some detail with co- and post-seismic slip by focusing on the southern end of the seismic gap, where our InSAR strain rate map is best resolved and where significant earthquakes occurred in 1995 and 2007 (Fig. 3). The upper limit of the 2007 M_w 7.7 Tocopilla earthquake rupture, which has broken north of the Mejillones Peninsula, is at ~30 km depth[18], and its trace at the Earth's surface is nearly coincident with the coastline. In our interseismic coupling models, this feature corresponds to the boundary between the shallow, rather-coupled (locked) zone and the deeper, less-coupled (partially locked) transition zone. South of the Mejillones Peninsula, the same depth separates regions with different behaviour: a locked upper zone that broke during the 1995 M_w 8.1 Antofagasta earthquake from a partially locked lower zone that underwent a 5-year aseismic afterslip pulse after the 1995 event, as well as intermediate magnitude (M_w 7–7.5) earthquakes[16,17]. The Mejillones Peninsula represents an anomaly in the trench–coastline distance. The structure of Mejillones is controlled by large N–S striking normal faults (~≥50 km along strike) that have uplifted Pleistocene marine terraces above sea level and that may extend down to the subduction plane with complex mechanical interactions[10]. The peninsula marks the boundary between two segments of the subduction: no past earthquake is known to have crossed this barrier[14], which instead localizes pulses of aseismic afterslip (after the 1995 and 2007 events; refs 16–18). Our results indicate that the subduction interface beneath the peninsula is only partially locked during the interseismic period, whereas it is highly coupled in both adjacent segments. Thus the seismogenic zone in North Chile seems segmented along-dip. The deeper transition zone (~30–50 km depth) under the landward forearc is partially locked during the interseismic period. It consists of a mosaic of regions that creep aseismically, intermixed with small seismic asperities. There, M_w 7–7.7 earthquakes (such as the 2007 Tocopilla event) can break ~30 × 30 km asperities, and trigger aseismic creep pulses surrounding these asperities during post-seismic or interseismic periods[16–18]. The shallow region (<30 km depth) under the oceanward forearc is locked during the interseismic period. It consists of large-scale asperities, which may break entirely during mega-thrust earthquakes, enabling rupture propagation downwards, well into the transition zone, and upwards to the trench[5,19,28].

It has been proposed that a change in dip in the seismogenic interface could explain the origin of both the N–S striking normal faults parallel to the coastal scarp and the observed along-dip segmentation[10]. That hypothesis seems to be supported by seismic refraction data that reveal an abrupt change in the dip of the subduction a few kilometres west of the coastline[15]. A model incorporating such a kink in the slab is consistent with our geodetic data (Fig. 3). That geometry could generate a damage zone

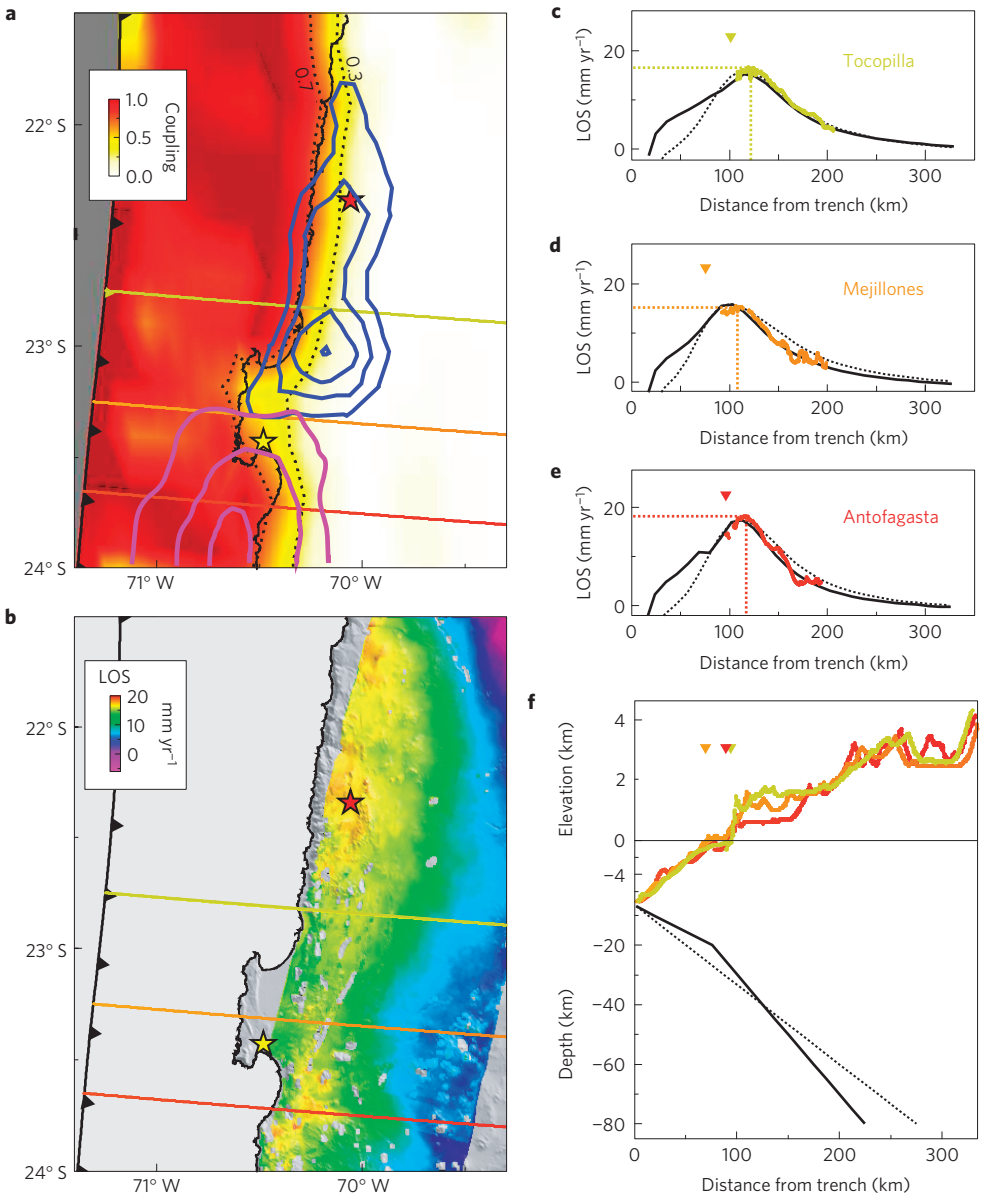

Figure 3 | Interseismic to coseismic behaviour around the Mejillones intersegment. a, Best coupling distribution inverted from cGPS and InSAR. Black dashed curves, iso-coupling 0.3 and 0.7. Pink and blue contours, coseismic slip distributions for 1995 M_w 8.1 Antofagasta (1, 2, 5 m) and 2007 M_w 7.7 Tocopilla (0.5, 1, 1.5 m) earthquakes, respectively. Stars, 1995 (yellow) and 2007 (red) epicentres. **b**, InSAR velocities. **c**–**e**, Profiles identified by colour in **a** and **b**. Coloured dots, measured LOS velocities. Coloured dashed lines, maximum velocity. Black curves, predicted LOS velocities (coastline parallel coupling) with planar (dashed) or kinked (solid) geometry. **f**, Black lines, planar and kinked geometries. Coloured lines, topographic profiles. Inverted triangles, coastline locations.

affecting the frictional behaviour of the subduction interface[9], acting as a geometric barrier to along-dip propagation of subduction earthquakes[29]. Over the long term, a ramp-flat geometry can promote localized underthrusting of crustal rocks and contribute to a thickening process causing the uplift of the Coastal Cordillera, thus also contributing to the growth of the Andes[10,24]. Regardless of geometric details, our coupling model with very fine correlation with coastline (Fig. 4) highlights the importance of similar structural features across forearcs elsewhere in the world[11,12,21] that seem to be steering the seismic properties of a variety of subduction plate interfaces.

Our results indicate that the North Chile seismic gap is currently accumulating significant elastic shortening that is likely to rebound in a future tsunamigenic megathrust earthquake breaking the whole seismogenic zone, from the trench to 55 km depth, releasing a moment deficit since the 1877 earthquake equivalent to magnitude $M_w \sim 8.6$ (see Supplementary Information). Regions of low coupling under Mejillones and possibly the Arica bend region can be regarded as potential barriers that may limit lateral propagation of rupture. Our results show an unambiguous relationship between the base of the interseismically coupled zone and the 1-km-high, 500-km-long coastal scarp that parallels the seismic gap. This observation is in stark contrast to models assuming a simple depth/temperature control on seismogenesis. A tectonic mechanism, persistent over several seismic cycles, must link processes occurring on the seismogenic

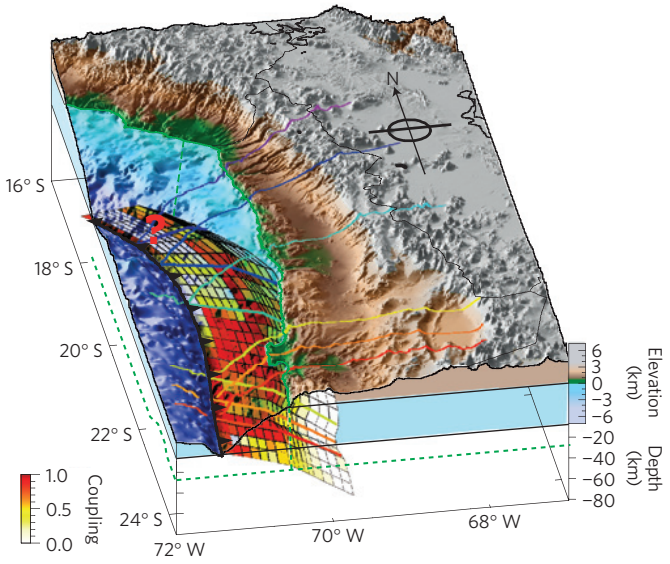

Figure 4 | 3D perspective showing the relationship between the coupling distribution and the coastal scarp. Shuttle Radar Topographic Mission topography is colour-coded as in Fig. 1. Yellow–red patches represent the coupling distribution on a kinked subduction interface. The shallow part (0–30 km depth) of the seismogenic zone is highly coupled and the deeper part (30–50 km depth) is partially coupled. The base of the coupling runs parallel to the coastal scarp. The resolution is poor north of 19° S (as indicated by the red question mark). Selected topographic profiles are shown together with their vertical projection on the slab. The colour code of the lines is function of latitude (same as in Fig. 1).

zone and tectonic processes involved in generation of topography in the Andean forearc.

Methods

Daily positions of GPS stations were estimated using the GAMIT software. We modelled cGPS time series as the sum of a linear trend, a Heaviside step function and a seasonal periodic signal to obtain horizontal and vertical velocities in each station. We compute the velocities with respect to the South American plate by applying a rigid rotation (see Supplementary Information).

InSAR velocities were estimated by building a stack of 18 interferograms processed with the ROI_PAC software suite (see Supplementary Fig. S5). The main limitation to extract the tectonic signal contained in InSAR measurements in this region comes from the presence of long-wavelength atmospheric and orbital signals in the interferograms that mimic the expected interseismic deformation. Orbital errors were corrected by removing a best-fit linear polynomial ramp from interferograms, using GPS velocities (projected in the LOS direction) as a reference. Phase propagation delays through the troposphere that change both with elevation and with distance to the coast[30] were corrected empirically, by estimating locally the delay to elevation relationship observed in interferograms. To avoid eliminating any long-wavelength deformation signal, the phase/elevation slope values are estimated at short wavelength, within small (10×10 km) sliding windows that span each interferogram (Supplementary Fig. S7). To reduce the local variability in the phase/topography slope values, we fit a 3° polynomial function of elevation. To evaluate the effectiveness of the corrections applied to interferograms, phase/elevation relationships were computed in the final stack and in modelled synthetic interferograms that contain only tectonic deformation. Although the tectonic model is correlated with the long-wavelength topography (that is, the phase/topography plot is not centred to zero but instead exhibits a small negative value), our correction method efficiently reduces the tropospheric delays by capturing the small wavelength correlations without removing the long-wavelength tectonic signal. Indeed, values of the phase/elevation slope in the stack are significantly reduced, centred around zero, and comparable to values present in a forward model (which only contains tectonic deformation), indicating that the atmosphere contribution has been successfully removed from our interferograms (Supplementary Table S2 and Fig. S8).

Forward and inverse elastic models of the measured velocity field are based on the back-slip asumption[25]. We have tested both a 2-plate model and a 3-plate model (that is, considering shortening in the Subandean regions by including an Andean sliver block between the Nazca and the South American plates). The coupling distribution pattern does not change between these two configurations, but we prefer the 3-plate model for the inversion as it reduces the GPS horizontal residuals in the eastern part of our region. We tested two different geometries of the megathrust, a uniformly dipping fault plane (15°) and a model incorporating a kink in the slab[15]. Both geometries explain the measured velocity field and provide similar results in terms of the location of the base of the coupled zone (Fig. 3). To invert for the coupling distribution, the megathrust interface is divided into 589 patches. The locking coefficient is obtained using a least-squares minimization with the non-negativity constraint. Slip direction is constant (parallel to the convergence), and the solution is regularized by minimizing the second-order derivative of the fault slip. In the joint inversion, relative weights between InSAR and cGPS data are tuned by searching for a compromise between the rms and the spatial density of each type of data. Inversion results for each data set are shown in Supplementary Fig. S18. The rate of moment deficit of our best model over the 1877 segment is 8.15×10^{19} N m yr^{-1} (assuming an averaged shear modulus of 33 GPa). If we assume this moment deficit rate is approximately steady since the 1877 rupture, it leads to a moment of 1.1×10^{22} N m, equivalent to a $M_w \sim 8.6$ event. See Supplementary Information for alternative models.

ENVISAT ASAR images used in this work can be requested from the European Space Agency (https://earth.esa.int/web/guest/pi-community/apply-for-data/full-proposal). CAnTO network cGPS data are available at http://tectonics.caltech.edu/resources/kmlandes.html and LIA-MdB network cGPS data at https://gpscope.dt.insu.cnrs.fr/chantiers/chili/.

Received 1 August 2012; accepted 19 March 2013; published online 28 April 2013

References

1. Scholz, C. H. Scaling laws for large earthquakes: Consequences for physical models. *Bull. Seismol. Soc. Am.* **72,** 1–14 (1982).
2. Ruegg, J. C. *et al.* Interseismic strain accumulation measured by GPS in the seismic gap between Constitucioń and Concepcioń in Chile. *Phys. Earth Planet. Inter.* **175,** 78–85 (2009).
3. Moreno, M., Rosenau, M. & Oncken, O. Maule earthquake slip correlates with pre-seismic locking of Andean subduction zone. *Nature* **467,** 198–202 (2010).
4. Loveless, J. P. & Meade, B. J. Spatial correlation of interseismic coupling and coseismic rupture extent of the 2011 $M_w = 9.0$ Tohoku-oki earthquake. *Geophys. Res. Lett.* **38,** L17306 (2011).
5. Chlieh, M. *et al.* Interseismic coupling and seismic potential along the Central Andes subduction zone. *J. Geophys. Res.* **116,** B12405 (2011).
6. Hetland, E. A & Simons, M. Post-seismic and interseismic fault creep II: Transient creep and interseismic stress shadows on megathrusts. *Geophys. J. Int.* **181,** 99–112 (2010).
7. Métois, M., Socquet, A. & Vigny, C. Interseismic coupling, segmentation and mechanical behaviour of the Central Chile subduction zone. *J. Geophys. Res.* **117,** B03406 (2012).
8. Kodaira, S. *et al.* Structural factors controlling the rupture process of a megathrust earthquake at the Nankai trough seismogenic zone. *Geophys. J. Int.* **149,** 815–835 (2002).
9. Wang, K. & Bilek, S. L. Do subducting seamounts generate or stop earthquakes? *Geology* **39,** 819–822 (2011).
10. Armijo, R. & Thiele, R. Active faulting in Northern Chile: Ramp stacking and lateral decoupling along a subduction plate boundary? *Earth Planet. Sci. Lett.* **98,** 40–61 (1990).
11. Song, T. R. A. & Simons, M. Large trench-parallel gravity variations predict seismogenic behavior in subduction zones. *Science* **301,** 630–633 (2003).
12. Wells, R. E., Blakely, R. J., Sugiyama, Y., Scholl, D. W. & Dinterman, P. A. Basin-centered asperities in great subduction zone earthquakes: A link between slip, subsidence, and subduction erosion? *J. Geophys. Res.* **108,** 2507 (2003).
13. Loveless, J. P., Pritchard, M. E. & Kukowski, N. Testing mechanisms of seismic segmentation with slip distributions from recent earthquakes along the Andean margin. *Tectonophysics* **495,** 15–33 (2010).
14. Comte, D. & Pardo, M. Reappraisal of great historical earthquakes in the northern Chile and southern Peru seismic gaps. *Nat. Hazards* **4,** 23–44 (1991).
15. Contreras-Reyes, E., Jara, J., Grevemeyer, I., Ruiz, S. & Carrizo, D. Abrupt change in the dip of the subducting plate beneath north Chile. *Nature Geosci.* **5,** 342–345 (2012).
16. Chlieh, M. *et al.* Crustal deformation and fault slip during the seismic cycle in the North Chile subduction zone, from Global Positioning System and InSAR observations. *Geophys. J. Int.* **158,** 695–711 (2004).
17. Pritchard, M. E. & Simons, M. An aseismic slip pulse in northern Chile and along-strike variations in seismogenic behavior. *J. Geophys. Res.* **111,** B08405 (2006).
18. Béjar-Pizarro, M. *et al.* Asperities, barriers and transition zone in the North Chile seismic gap: State of the art after the 2007 M_w 7.7 Tocopilla earthquake inferred by GPS and InSAR data. *Geophys. J. Int.* **183,** 390–406 (2010).
19. Vigny, C. *et al.* The 2010 M_w 8.8 Maule Megathrust Earthquake of Central Chile, Monitored by GPS. *Science* **332,** 1417–1421 (2011).

20. Singh, S. C. *et al.* Aseismic zone and earthquake segmentation associated with a deep subducted seamount in Sumatra. *Nature Geosci.* **4,** 308–311 (2011).
21. Fuller, C. W., Willett, S. D. & Brandon, M. T. Formation of forearc basins and their influence on subduction zone earthquakes. *Geology* **34,** 65–68 (2006).
22. Vigny, C. *et al.* Upper plate deformation measured by GPS in the Coquimbo Gap, Chile. *Phys. Earth Planet. Int.* **175,** 86–95 (2009).
23. Armijo, R. *et al.* The West Andean Thrust, the San Ramón Fault, and the seismic hazard for Santiago, Chile. *Tectonics* **29,** TC2007 (2010).
24. Adam, J. & Reuther, C. D. Crustal dynamics and active fault mechanics during subduction erosion. Application of frictional wedge analysis on to the North Chilean Forearc. *Tectonophysics* **321,** 297–325 (2000).
25. Savage, J. A dislocation model of strain accumulation and release at a subduction zone. *J. Geophys. Res.* **88,** 4984–4996 (1983).
26. Bevis, M. *et al.* On the strength of interplate coupling and the rate of back arc convergence in the central Andes: An analysis of the interseismic velocity field. *Geochem. Geophys. Geosyst.* **2,** GC000198 (2001).
27. Khazaradze, G. & Klotz, J. Short- and long-term effects of GPS measured crustal deformation rates along the south central Andes. *J. Geophys. Res.* **108,** 2289 (2003).
28. Simons, M. *et al.* The 2011 Magnitude 9.0 Tohoku-Oki earthquake: Mosaicking the megathrust from seconds to centuries. *Science* **322,** 1421–1425 (2011).
29. Wesnousky, S. G. Predicting the endpoints of earthquake ruptures. *Nature* **444,** 358–360 (2006).
30. Fournier, T. J., Pritchard, M. E. & Finnegan, N. J. Accounting for atmospheric delays in InSAR data in a search for long wavelength deformation in South America. *IEEE Trans. Geosci. Remote Sens.* **49,** 3856–3867 (2011).

Acknowledgements

This work was performed in the frame of the French/Chilean international collaboration (CNRS/CONICYT LIA 'Montessus de Ballore'). We thank the European Space Agency (ESA) for providing the ENVISAT images (project AO-720). This work was made possible thanks to the funding of the French National Research Agency (ANR-05-CATT-014, ANR-06-CATT-010-01), CNRS/INSU PNTS project, BQR IPGP and the LABEX UnivEarthS (Sorbonne Paris Cité, IPGP). Development and analysis of the CAnTO GPS network was partly supported by the Gordon and Betty Moore Foundation. We are very grateful to the many people who contributed to the development and maintenance of the permanent GPS network in North Chile and the associated database, in particular C. Aranda, S. Barrientos, J. Campos, J. B. de Chabalier, O. Charade, D. Comte, A. Delorme, B. Glass, J. Galetzka, E. Maureira, A. Nercessian, M. Olcay, I. Ortega, J. C. Ruegg, C. Valderas-Bermejo and C. Vigny.

Author contributions

M.B-P. processed InSAR data, analysed InSAR and cGPS time-series, and did the modelling. A.S. designed the study, collected the GPS data, and supervised geodetic analysis and modelling. R.A. did the geomorphologic analysis and geological interpretation. D.C. collected the GPS data and contributed to the geological interpretation. J.G. collected and processed GPS data. M.S. contributed to the data collection, geodetic analysis and modelling. The paper was co-written by A.S., R.A. and M.B-P. All authors discussed the results and commented on the paper.

Additional information

Supplementary information is available in the online version of the paper. Reprints and permissions information is available online at www.nature.com/reprints. Correspondence and requests for materials should be addressed to M.B-P.

Competing financial interests

The authors declare no competing financial interests.